Development of chopper-stabilized ASIC preamplifier for improving noise equivalent magnetic induction of search coil magnetometer probing space plasma waves

Mitsunori Ozaki[1*], Yuya Tokunaga[1,2], Hiroki Koji[1] and Satoshi Yagitani[1]

Abstract

Space-based search coil (SC) magnetometers connected to preamplifiers have been used to investigate magnetic field vectors of plasma waves from 100 mHz to 10 kHz for understanding magnetospheric dynamics. However, flicker noise below several 100 Hz of typical preamplifiers degrades the noise equivalent magnetic induction (NEMI) of SCs and affects the probing of plasma waves from 100 mHz to 100 Hz. In this study, we developed a chopper-stabilized preamplifier using application-specific integrated circuit (ASIC) technology for improving the NEMI below 100 Hz while maintaining miniaturization and a low power consumption. The chopper ASIC preamplifier fits into a layout size of 2.3✕3.4 mm in a bare chip. We used two SC sensors with different (20 cm and 5 cm) lengths to evaluate the NEMI with the prototype of the chopper ASIC preamplifier. At 100 mHz, the NEMI values of the 20-cm length and 5-cm length SCs were 0.1 nT/Hz$^{1/2}$ and 1.9 nT/Hz$^{1/2}$, respectively, which can detect typical electromagnetic ion cyclotron waves in the magnetosphere. The NEMI value at 100 mHz for the 5-cm-length SC was improved by approximately 19 dB compared with that for a previous ASIC preamplifier without chopping. We conducted temperature tests for the chopper ASIC preamplifier to evaluate the behavior for under a wide temperature range from − 40 to + 100 ℃. The temperature coefficient of the gain was approximately − 0.02 dB/℃, which is a sufficiently low temperature-dependence. The use of ASIC technology achieved high stability under the wide temperature range and radiation tolerance. Thus, the chopper ASIC preamplifier with high robustness and ultra-low noise characteristics is suitable for plasma wave observations in harsh space environments for future missions.

Keywords Search coil magnetometer, Application-specific integrated circuit, Chopper amplifier, Miniaturized instruments, Plasma wave
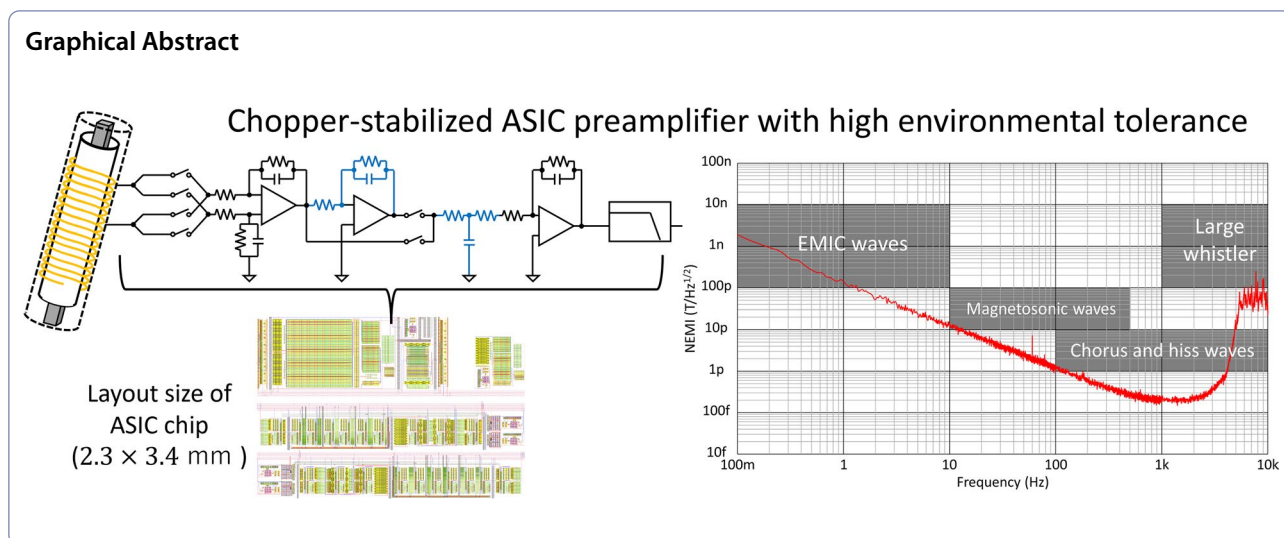
*Correspondence:
Mitsunori Ozaki
ozaki@is.t.kanazawa-u.ac.jp
Full list of author information is available at the end of the article

Ozaki *et al. Earth, Planets and Space*   (2023) 75:84

Page 2 of 11

Graphical Abstract

Chopper-stabilized ASIC preamplifier with high environmental tolerance

Layout size of ASIC chip
(2.3 × 3.4 mm)

Introduction

Demands for miniaturized scientific satellites are increasing, so miniaturization of scientific instruments is important for understanding spatial and temporal magnetospheric dynamics using cube- and small-satellites (e.g., Angelopoulos et al. 2020; Johnson et al. 2020; Walsh et al. 2021). Plasma wave instruments have been miniaturized by application-specific integrated circuit (ASIC) technology (e.g., direct current (DC) magnetic field measurements (Magnes et al. 2008; Sordo-Ibáñez et al. 2015), alternating current (AC) magnetic field measurements (Rhouni et al. 2013; Ozaki et al. 2014; Ozaki et al. 2016), and plasma waveform receivers (Kojima et al. 2010; Fukuhara et al. 2012; Zushi et al. 2015)). ASIC technology is suitable for miniaturizing mostly analog parts for plasma wave observations. In this study, we focus on AC magnetic field measurements of plasma waves from 100 mHz to 10 kHz using search coil (SC) magnetometers. The noise equivalent magnetic induction (NEMI) of an SC is an important property for determining the detectable frequency range of magnetic field intensities. However, a complementary metal oxide semiconductor (CMOS) preamplifier has flicker noise that directly affects the NEMI below 100 Hz. A chopper-stabilized preamplifier displays ultra-low noise characteristics in the frequency range below 100 Hz (Yan et al. 2014), but the circuit size will be large because of modulation and demodulation components. We have developed a chopper-stabilized preamplifier with tiny size and high robustness for space environments using ASIC technology to improve the NEMI from 100 mHz to 100 Hz. We analyzed an equivalent circuit model for analytically evaluating the NEMI of an SC with the chopper ASIC preamplifier.

This study presents the basic design of the chopper ASIC preamplifier and demonstrates the electrical performances of its prototype in laboratory experiments.

Chopper ASIC preamplifier for SC

Figure 1a, b shows a schematic circuit diagram of an SC with a chopper ASIC preamplifier, and the outlines of output voltage spectra at each circuit stage, respectively. The blue components in Fig. 1a are external resistances and capacitances outside of the bare chip. The circuit parameters of the chopper ASIC preamplifier are listed in Table 1. In this study, we deal with a one-axis SC and a one-channel chopper ASIC preamplifier for simplification. The chopper ASIC preamplifier consists of five stages (i)–(v), as shown in Fig. 1a. Stages (i) and (iii) are a modulator and a demodulator, respectively, which consist of the CMOS switches SW_1 and SW_2. Each switch has an on-resistance R_{SW} of 370 Ω. A clock signal and another clock signal reversed by an inverter control the on−off state of SW_1 and SW_2, respectively. The demodulator is based on an inverting amplifier. Stage (ii) is a low-noise ASIC amplifier that amplifies the modulated signal. The circuit structure of the ASIC preamplifier in stage (ii) is the same to that of Ozaki et al. (2016) for the current sensing. The gain adjustment amplifier of stage (iv) adjusts the gain by the external resistance R_6. The external resistance R_5 and capacitance C_3 in the gain adjustment amplifier are used to add a first-order low-pass filter (LPF). Stage (v) as a noise reduction filter from the clock signals is a 12th-order Chebyshev LPF, which is consisted of an analog front end ASIC by Tokunaga et al. (2020). All the circuits of the chopper ASIC preamplifier (except for the external resistances R_3 to R_6 and capacitances C_2 and C_3) were developed by a standard 0.25-μm

(a) Circuit diagram of chopper ASIC preamplifier

(b) Outlines of output voltage spectra at each stage
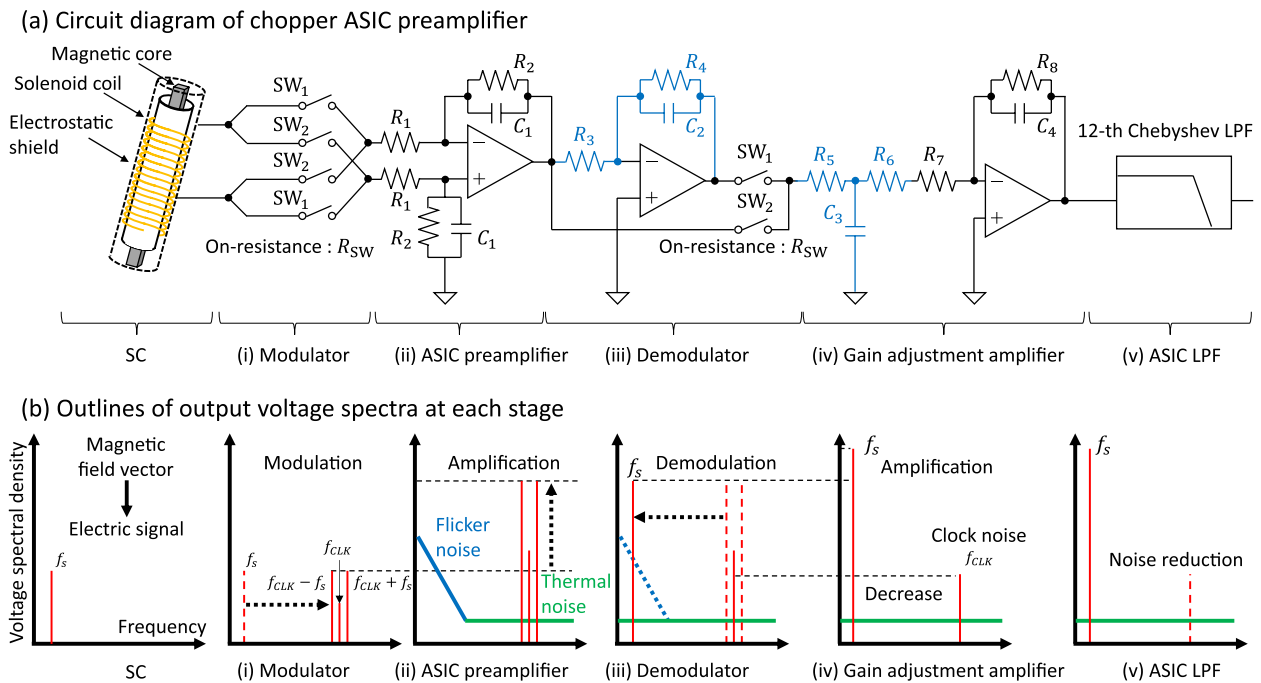
Fig. 1 Circuit diagram of **a** the chopper ASIC preamplifier for SC magnetometer, and **b** outlines of output voltage spectra at each circuit stage

**Table 1** Circuit parameters of the chopper ASIC preamplifier

Parameter	Value	Unit
On-resistance of CMOS switch R_{SW}	370	Ω
R_1	0.9	kΩ
R_2, R_8	0.98	MΩ
R_3, R_4	100	kΩ
R_5	22	kΩ
R_6	68	kΩ
R_7	9.8	kΩ
C_1, C_4	1.6	pF
C_2	6.8	pF
C_3	4.7	nF

CMOS process. The input resistance R_3, feedback resistance R_4, and capacitance C_2 of the inverting amplifier in the demodulator were not embedded in the ASIC chip and were adjusted after developing the chopper ASIC preamplifier to allow adjustment of different SC sensors. Figure 2 shows the whole layout of the chopper ASIC preamplifier. The layout size of the chopper ASIC preamplifier fits into 2.3×3.4 mm in a bare chip.

The operating principles of the chopper ASIC preamplifier with an SC can be described as follows. From Fig. 1b, an AC magnetic field vector of a plasma wave is converted into a weak (μV to mV) electrical signal by the

SC following Faraday's law of electromagnetic induction. In stage (i), the weak signal at frequency f_s is modulated by the clock signal at f_{CLK}. The frequencies of the modulated signal range from $f_{CLK} - f_s$ and $f_{CLK} + f_s$, where the relationship between f_{CLK} and f_s is $f_{CLK}/2 \gg f_s$. In stage (ii), the ASIC preamplifier amplifies the modulated signal in the frequency range of thermal noise. The thermal noise floor is usually much lower than the flicker noise of the ASIC preamplifier in stage (ii). The input signal below $f_{CLK}/2$ converted to around f_{CLK} by chopping is mitigated from the effects of the flicker noise of the ASIC preamplifier. In stage (iii), the amplified modulation signal is demodulated to the original frequency range, but the clock noise at f_{CLK} remains. In stage (iv), the gain adjustment amplifier increases the gain and suppresses the clock noise. In stage (v), the ASIC LPF decreases the clock noise coming from chopping. The measurement frequency range is especially characterized with the gain band width product of the ASIC preamplifier in stage (ii) to amplify the modulation signals with the flat gain in the frequency range from $f_{CLK} \pm f_s$. We set f_{CLK} as 10 kHz and the cut-off frequency of the ASIC LPF as 4 kHz.

The NEMI is defined as the minimum detectable intensity of the magnetic field vector. An SC with a lower NEMI expands the detectable frequency range for plasma wave observations. We obtain the NEMI as the ratio of the output noise voltage E_{OUT} to the magnetic gain G, where G is defined as the output voltage of the chopper ASIC

Ozaki *et al. Earth, Planets and Space*   (2023) 75:84

Page 4 of 11
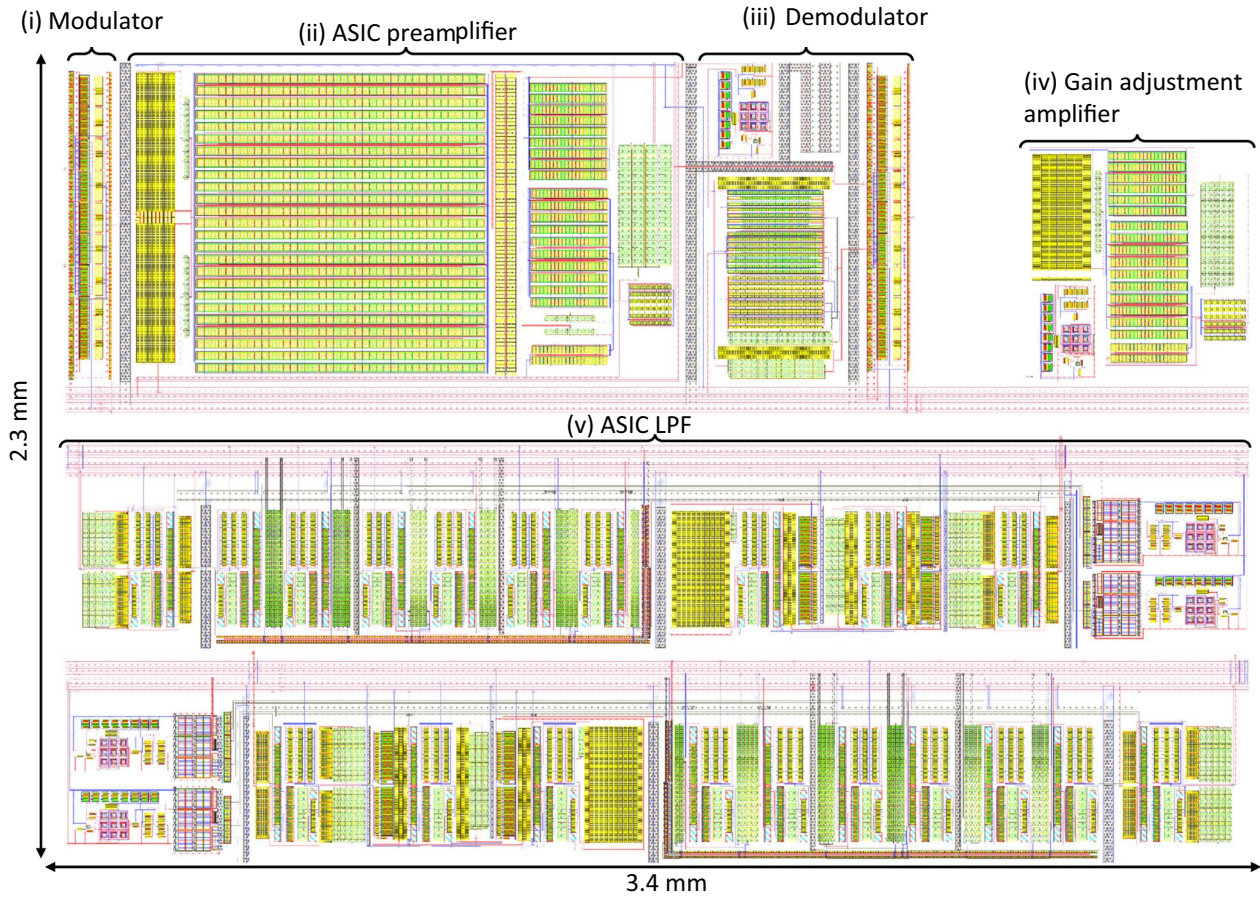
Fig. 2 Layout of the chopper ASIC preamplifier

preamplifier per input magnetic flux to the SC. Figure 3 shows an equivalent circuit model for the SC with the chopper ASIC preamplifier. The equivalent circuit of the SC is expressed by an *RLC* resonance circuit, where *R*, *L*,

and *C* are the resistance, inductance, and parasitic capacitance of the SC sensor, respectively. In the equivalent circuit model, E_{SC}, E_{IN}, and E_{FB} are thermal noises generated by the resistances R, $(R_{SW} + R_1)$, and R_2, respectively. E_{OP} is an equivalent input noise at 10 kHz of the ASIC preamplifier with the open-loop configuration for stage (ii). E_{OUT} is an output noise of the chopper ASIC preamplifier. I_{CHOP} is a current noise from the charge injection to the input caused by chopping (Xu et al. 2013). Parameters of Z_{RL}, Z_C, Z_{IN}, and Z_{FB} are impedances for $R + j\omega L$, $1/j\omega C$, $R_{SW} + R_1$, and $R_2 || (1/j\omega_{CLK} C_1)$, respectively. ω is an

angular frequency, ω_{CLK} is for clock frequency calculated by $2\pi(f_{CLK} - f)$, and Z_{FB} is also calculated at $\omega_{CLK} - \omega$ because of the circuit operation between the modulator and demodulator. The output noise of the chopper ASIC preamplifier E_{OUT} can be represented as:

$$E_{OUT} = \sqrt{\left|E_{SC\_O}\right|^2 + 2\left|E_{IN\_O}\right|^2 + 2\left|E_{FB\_O}\right|^2 + \left|E_{OP\_O}\right|^2 + 2\left|E_{I\_O}\right|^2}, \tag{1}$$

where E_{SC_O}, E_{IN_O}, E_{FB_O}, E_{OP_O}, and E_{I_O} are output noises converted from the noise sources E_{SC}, E_{IN}, E_{FB}, E_{OP}, and I_{CHOP}, respectively. Each output noise is expressed as follows:

$$E_{SC\_O} = -Z_{FB} \frac{2Z_C}{Z_{RL}Z_C + 2Z_{RL}Z_{IN} + 2Z_C Z_{IN}} E_{SC}, \tag{2}$$

$$E_{IN\_O} = -Z_{FB} \frac{2Z_{RL} + 2Z_C}{Z_{RL}Z_C + 2Z_{RL}Z_{IN} + 2Z_C Z_{IN}} E_{IN}, \tag{3}$$

$$E_{FB\_O} = E_{FB}, \tag{4}$$
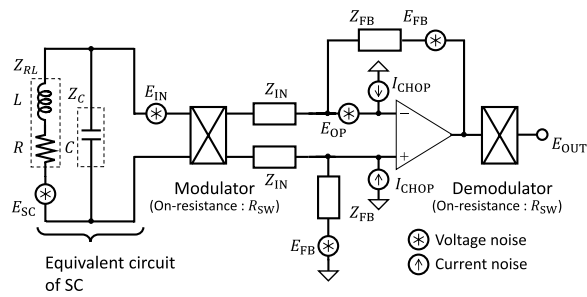
Fig. 3 Equivalent circuit model of the chopper ASIC preamplifier connected to an SC

$$E_{\mathrm{OP\_O}} = \left(1 - Z_{\mathrm{FB}} \frac{2Z_{\mathrm{RL}} + 2Z_C}{Z_{\mathrm{RL}}Z_C + 2Z_{\mathrm{RL}}Z_{\mathrm{IN}} + 2Z_C Z_{\mathrm{IN}}}\right) E_{\mathrm{OP}}, \quad (5)$$

$$E_{I\_O} = -Z_{\mathrm{FB}} I_{\mathrm{CHOP}}. \qquad (6)$$

The magnetic gain $|G|$ is represented as:

$$|G| = \left| -Z_{\mathrm{FB}} \frac{2Z_C}{Z_{\mathrm{RL}}Z_C + 2Z_{\mathrm{RL}}Z_{\mathrm{IN}} + 2Z_C Z_{\mathrm{IN}}} \cdot e \right|, \qquad (7)$$

where

$$e = -j\omega NBS\mu_{\mathrm{eff}} \qquad (8)$$

is the induced voltage of SC, N is the number of windings, B is an external magnetic field parallel to a cross section of the magnetic core, and S and μ_{eff} are a cross-sectional area and effective permeability of the magnetic core, respectively. From Eqs. (1) and (8), the NEMI B_{NEMI}

of the SC connected to the chopper ASIC preamplifier is given by:

$$B_{\mathrm{NEMI}} = \frac{E_{\mathrm{OUT}}}{|G|}. \qquad (9)$$

Finally, we can analytically obtain the B_{NEMI} of the SC with the chopper ASIC preamplifier from Eq. (9).

Electrical characteristics of chopper ASIC preamplifier
We evaluated electrical characteristics of the chopper ASIC preamplifier using prototype ASIC chips, which are divided into each circuit block for actual measurements with plastic packaging. Figure 4 shows the measurement and calculation results of the gain response for the chopper ASIC preamplifier. The measured gain is 77 dB from 10 mHz to 500 Hz. The ratios of R_2 to $(R_{\mathrm{SW}} + R_1)$ and R_8 to $(R_{\mathrm{SW}} + R_5 + R_6 + R_7)$ in Fig. 1a determine the flat gain of the chopper ASIC preamplifier. The external LPF of R_5 and C_3 has a cut-off frequency of 1.5 kHz. The 12th-order Chebyshev ASIC LPF gives a 0.4 dB ripple at a cut-off frequency of approximately 4 kHz.

Figure 5 shows the equivalent input noise of the chopper ASIC preamplifier, the ASIC preamplifier in stage (ii), and the inverting amplifier of the demodulator in stage (iii). The average values of the measured equivalent input noise from 100 Hz to 1 kHz for the ASIC preamplifier in stage (ii) and the chopper ASIC preamplifier are 7.31 and 8.57 nV/Hz$^{1/2}$, respectively. The thermal noise of the chopper ASIC preamplifier can be approximately calculated from $\sqrt{8k(R_1 + R_{\mathrm{SW}})T + E_{\mathrm{OP}}^2}$, where k is the Boltzmann constant, T is an ambient temperature, and
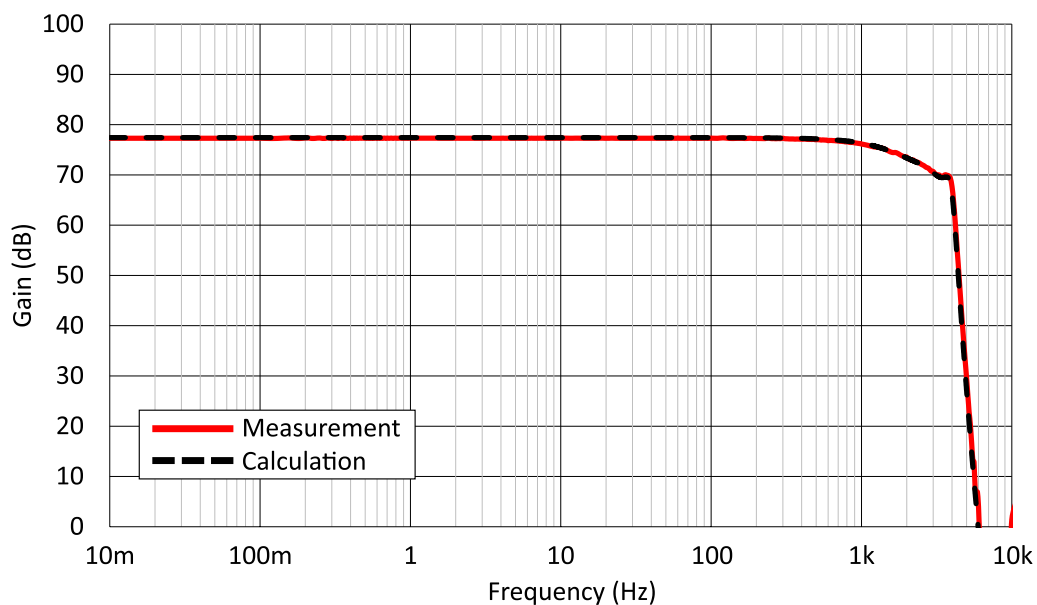

Fig. 4 Measured (red solid line) and calculated (black dashed line) gain responses for the chopper ASIC preamplifier

Ozaki *et al. Earth, Planets and Space*   (2023) 75:84

Page 6 of 11
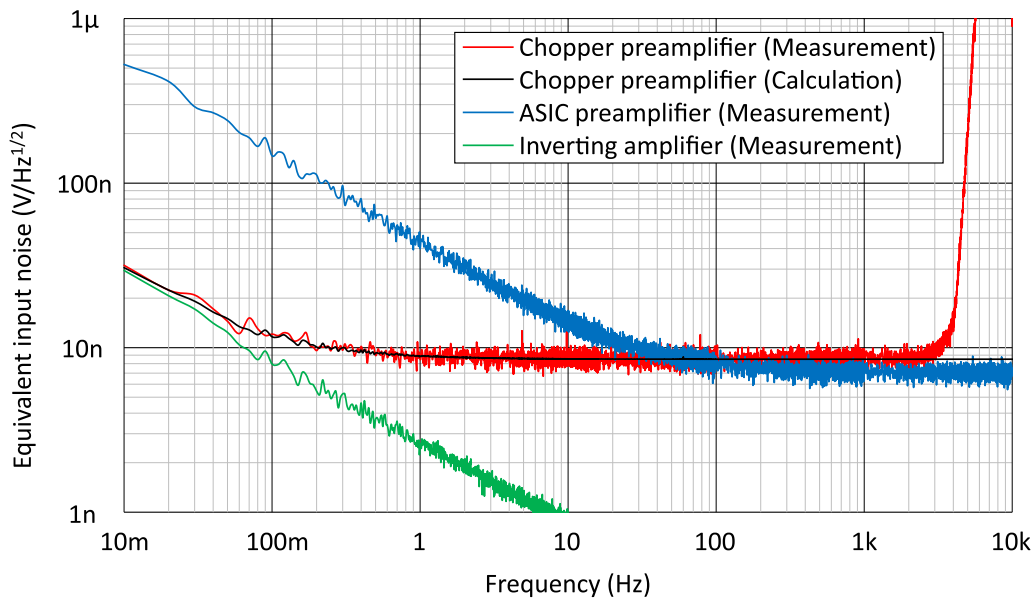
Fig. 5 Measured (red, blue, and green solid lines) and calculated (black solid line) equivalent input noise results for the chopper ASIC preamplifier, ASIC preamplifier in stage (ii), and demodulator in stage (iii)

E_{OP} is an equivalent input noise of the ASIC preamplifier in stage (ii), because the input resistances are the dominant components. Parameters of R_1 and $R_1 + R_{SW}$ are doubled due to the fully differential input of the ASIC preamplifier. The difference in the thermal noise between the ASIC preamplifier in stage (ii) (7.31 nV/Hz$^{1/2}$) and the chopper ASIC preamplifier (8.57 nV/Hz$^{1/2}$) is caused by the additional noise coming from R_{SW}. The measurement results of the chopper ASIC preamplifier show flicker noise from 10 mHz to 1 Hz. The flicker noise is caused by the demodulator consisting of an inverting amplifier including flicker noise that is larger than the output noise after the modulation. The equivalent input noise of the chopper ASIC preamplifier in the black line was calculated by $\sqrt{E_{AMP}^2 + E_{OP}^2 + 8k(R_1 + R_{SW})T}$, where E_{AMP} is an equivalent input noise of the inverting amplifier shown by the green line in Fig. 5. In the calculation in Fig. 5, we estimated E_{OP} from 100 Hz to 100 kHz as 5.5 nV/Hz$^{1/2}$ by the measured results. The flicker noise is large under 100 mHz due to the noise property from the demodulator by the inverting amplifier, so we think that the observation frequency range of the plasma waves is suitable above 100 mHz in this chopper ASIC preamplifier. The steep increase above 4 kHz of the equivalent input noise is caused by the noise characteristics of the 12th-order Chebyshev ASIC LPF in stage (v). The equivalent input noise of the chopper ASIC preamplifier is approximately 21 dB lower than that of the ASIC preamplifier in stage (ii) at 100 mHz.

Figure 6a, b shows the output waveforms of the chopper ASIC preamplifier when applying sine waves at 10 Hz and 2 kHz, respectively. The figures show that there is no 10 kHz clock noise coming from the modulator and demodulator because it is reduced from 30 mV/Hz$^{1/2}$ to 5 µV/Hz$^{1/2}$ before and after the ASIC LPF in stage (v). Figure 6c, d shows the spectra of the output waveforms applied to sine waves at 10 Hz and 2 kHz, respectively, to measure the total harmonic distortion (THD). The THD is defined as the fundamental spectrum divided by the second or third harmonics, whichever is larger. The THD values at 10 Hz and 2 kHz are 56.5 dB and 61.0 dB, respectively. The external LPF with a 1.5 kHz cut-off frequency decreased the second harmonic generated by the fundamental spectrum at 2 kHz. The ripple effect around approximately 4 kHz comping from the Chebyshev ASIC LPF in stage (v) to the output waveform is sufficiently small. The output dynamic range of the chopper ASIC preamplifier is 2.96 Vpp at 10 Hz and 2.80 Vpp at 2 kHz while maintaining a 40 dB THD. The chopper ASIC preamplifier outputs a waveform at over 80% of the 3.3-V supply voltage with a low distortion. The evaluation results of the electric characteristics show the chopper ASIC preamplifier can probe accurate amplitudes of plasma waves over the frequency range including the flicker noise. The power consumption of the chopper ASIC preamplifier is 53.8 mW. If we consider three-channel chopper ASIC preamplifiers for three-axis
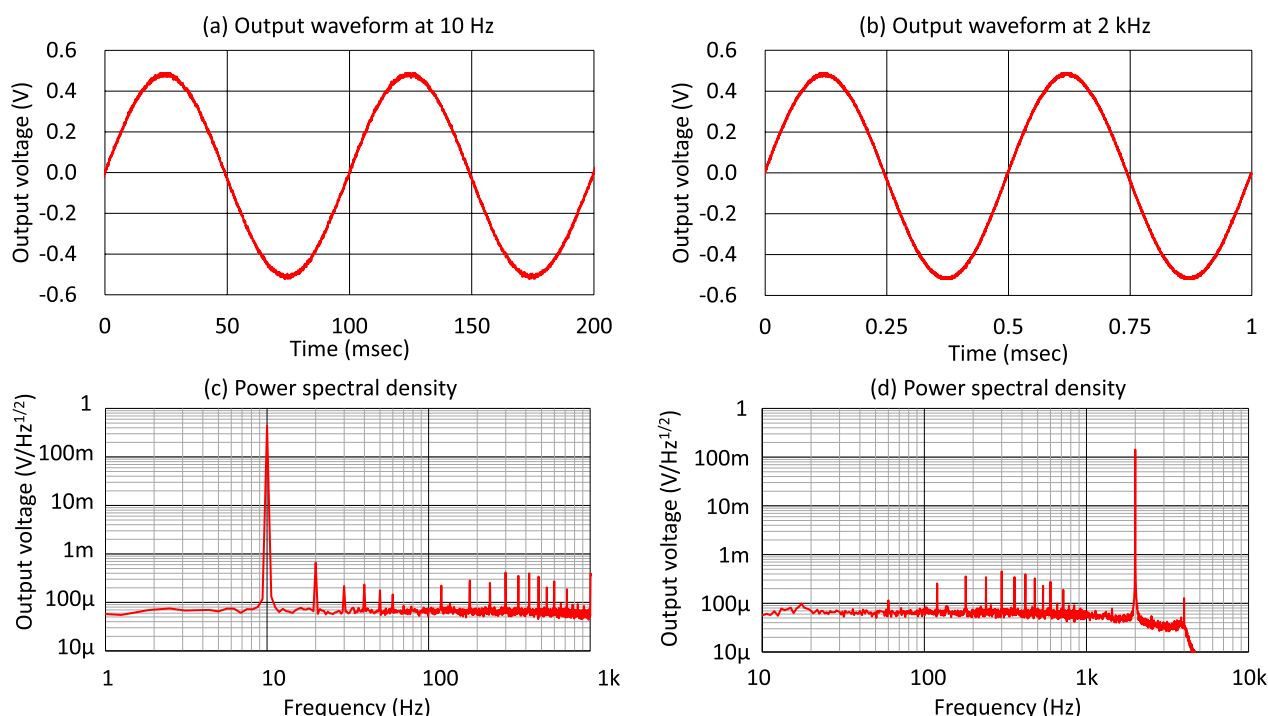
Fig. 6 Measured output waveforms at **a** 10 Hz and **b** 2 kHz of the chopper ASIC preamplifier, and their power spectral densities at **c** 10 Hz and **d** 2 kHz

SC sensors to detect magnetic field vectors in a three-dimensional space, the total power consumption is 161.4 mW, which is 62.5% lower than the 430-mW power consumption of the three-channel preamplifiers for the Arase satellite (Ozaki et al. 2018). The chopper ASIC preamplifier can contribute to the reduction of the power consumption using CMOS integrated circuits instead of bipolar operational amplifiers.

Evaluation of NEMI

We prepared prototype SCs having magnetic cores of 20-cm and 5-cm lengths, as shown in Fig. 7, to evaluate the NEMI when connected to the chopper ASIC preamplifier for future missions by a small ($50 \times 50 \times 50$ cm) satellite and a 1U cube ($10 \times 10 \times 10$ cm) satellite. The parameters of both SC sensors are listed in Table 2. The parasitic capacitance of a 5-m harness connecting both SC sensors and the chopper ASIC preamplifier is larger than the parasitic capacitance of both SC sensors. The NEMI depends on the length of the SC, because a shorter SC has a lower effective permeability μ_{eff}. From Eqs. (7) and (8), the magnetic gain G of the 5-cm length SC is lower than that of the 20-cm length SC because of the smaller μ_{eff}. The chopper ASIC preamplifier with ultra-low noise (12 nV/Hz$^{1/2}$ at 100 mHz) characteristics in Fig. 5 compensates for the insufficient G for the 5-cm length SC.
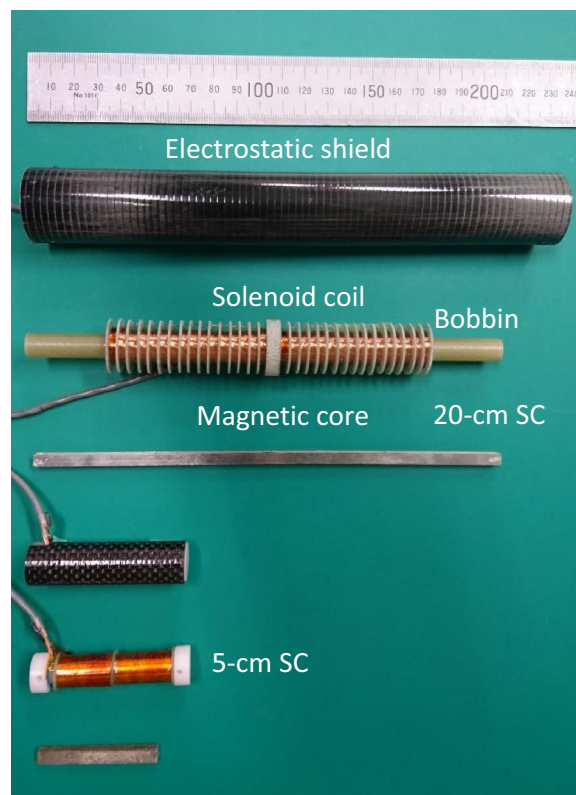
**Fig. 7** Photograph of 20-cm length and 5-cm length SCs

Ozaki *et al. Earth, Planets and Space*   (2023) 75:84

Page 8 of 11

Table 2 Parameters of 20-cm and 5-cm SC sensors

Parameter	20-cm SC	5-cm SC	Unit
Resistance of coil R	1.39	1.48	kΩ
Inductance of coil L	20.1	2.7	H
Parasitic capacitance of coil and 5-m harness C	1.00		nF
Number of windings of coil N	14,000	10,000	turns
Cross-sectional area of magnetic core S	5×5		mm^2
Effective permeability of magnetic core μ_{eff}	452	50	

Figure 8 shows the NEMI of the 20-cm SC connected to the preamplifiers. The green line is for a flux gate magnetometer of the Arase satellite referred from Matsuoka et al. (2018). The gray areas in Fig. 8 show the spectral density of typical plasma waves for reference. The calculation result by the equivalent circuit model (Fig. 3) using Eq. (9) is in good agreement with the measured result. The measured NEMI above 1 Hz was better than that of the flux gate magnetometer by the Arase satellite. The NEMI above 100 mHz of the 20-cm SC is lower than a value of 80 pT/Hz$^{1/2}$ (purple line), which is a mission requirement of the flux gate of the Arase satellite (Matsuoka et al. 2018). The Arase satellite measured the electromagnetic ion cyclotron (EMIC) waves mainly by the flux gate, but the 20-cm SC with the chopper ASIC preamplifier is detectable for EMIC waves. Therefore, we can conduct a complementary measurement for probing EMIC waves using the flux gate and SC powered by the developed chopper ASIC preamplifier to cover the wider frequency band. Such complementary measurements for probing EMIC waves using flux gate and SC magnetometers should contribute to a quantitative assessment of atmospheric impacts on energetic particle precipitation driven by EMIC waves (Ozaki et al. 2022) and behaviors of unusual high frequency EMIC waves (Teng et al. 2019).

The NEMI of the 5-cm SC with the chopper ASIC preamplifier, as shown in Fig. 9, was also improved by 19.1 dB at 100 mHz compared with that of the ASIC preamplifier in stage (ii) with the 5-cm SC. The chopper ASIC preamplifier is suitable for conducting plasma wave observations from 100 mHz to 4 kHz, even by the 5-cm SC for a 1U cube satellite. In the frequency range above 500 Hz, the output noise E_{I_O} from the current noise I_{CHOP} dominates the NEMI in the chopper ASIC preamplifier. The main reason is coming from charge injection by chopping generating I_{CHOP} (Xu et al. 2013). From the measurement results, we estimated that I_{CHOP} is approximately 900 fA/Hz$^{1/2}$. Although the NEMI of the chopper ASIC preamplifier with the 5-cm length SC was degraded by the effects of the charge injection in comparison with a NEMI by the 5-cm SC with the ASIC preamplifier in stage (ii) with no chopping, it is sufficient to cover the spectral densities of typical plasma waves such as chorus and hiss waves, which can contribute to acceleration and loss of radiation belt electrons (e.g., Baker 2021; Omura 2021). From the measurement results in Figs. 8 and 9, we consider that the chopper ASIC preamplifier is an acceptable solution for improving the NEMI.
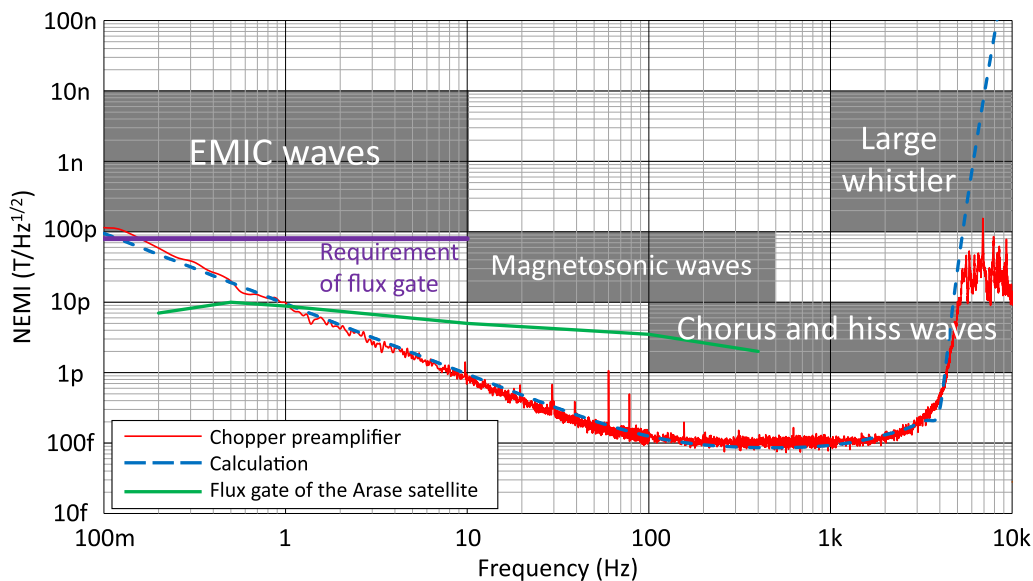
Fig. 8 NEMI curves of the 20-cm SC connected to the chopper ASIC preamplifier (red line); calculation results (blue dashed line) for the chopper ASIC preamplifier, and flux gate (green line) of the Arase satellite. Gray areas indicate typical spectral densities of plasma waves

Ozaki *et al. Earth, Planets and Space* (2023) 75:84

Page 9 of 11
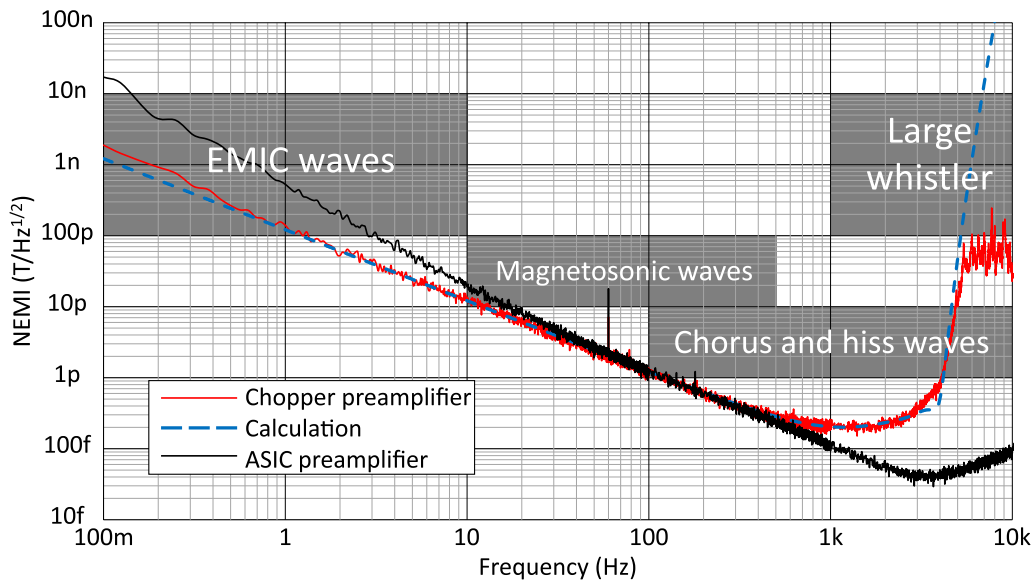
Fig. 9 NEMI curves of the 5-cm SC connected to the chopper ASIC preamplifier (red line) and ASIC preamplifier (black line), calculation results (blue dashed line) for the chopper ASIC preamplifier, and typical spectral densities of plasma waves (gray areas)

Environmental tolerance

Plasma wave instruments should be insensitive to ambient temperature to accurately measure the amplitude of plasma waves. Tokunaga et al. (2020) performed temperature tests for analog front end ASIC, which use the same CMOS process as the chopper ASIC preamplifier in this study, over a range from -60 to $+100$ °C to confirm their temperature stability. Their results showed a low-temperature dependence for space

experiments. Temperature tests for the chopper ASIC preamplifier were conducted in a thermostatic chamber (ETAC FL420N, Kusumoto Chemicals, Ltd.) at Kanazawa University. In particular, the chopper ASIC preamplifier is designed using a proportional to absolute temperature (PTAT) reference voltage generator (Brokaw 1974; Ozaki et al. 2016) for all amplifiers in the chip to achieve a wide operating temperature range. We evaluated the electrical characteristics of the chopper
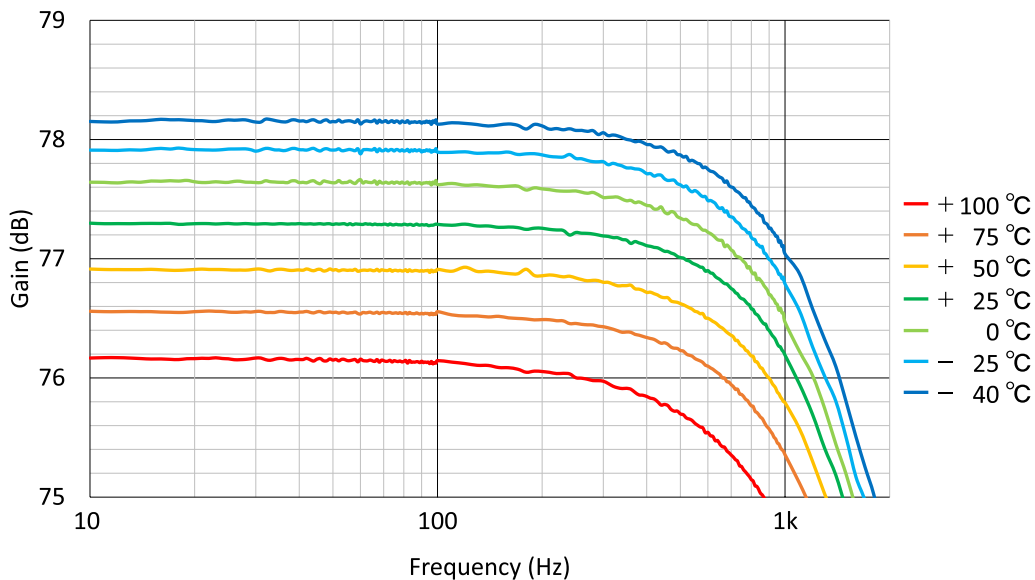
Fig. 10 Measured gain response results at each temperature for the chopper ASIC preamplifier during temperature tests

Ozaki *et al. Earth, Planets and Space* (2023) 75:84

Page 10 of 11

ASIC preamplifier without connecting the SC to avoid detecting the facility noise from the thermal chamber. The temperature ranged from -40 to $+100$ °C owing to the minimum chamber temperature of -40 °C.

Figure 10 shows the gain response of the chopper ASIC preamplifier at each temperature. The temperature coefficients of the gain at 100 Hz and 1 kHz are -1.4×10^{-2} and -1.6×10^{-2} dB/°C, respectively. The gain variation from -40 to $+100$ °C is within 2.0 dB. We performed a temperature simulation for the chopper ASIC preamplifier using a circuit simulator (Tanner EDA). From the simulation results, the variation of the gain in the temperature range from -40 to $+100$ °C was within 1.0 dB.

The equivalent input noise in the frequency range (10 Hz–10 kHz) was also measured and showed almost constant for temperature in comparison with Fig. 5 for a room temperature. The frequency range of the measured equivalent input noise was 10 Hz–10 kHz in order to save testing time. From the averages at -40 and $+100$ °C, the variation of the equivalent input noise was approximately 1.65 dB within the temperature range. During the temperature tests, the output dynamic range at 10 Hz and 2 kHz was also evaluated. Both output dynamic ranges kept over 80% at a 3.3 V supply voltage. The variation of the output offset voltage was under ± 100 mV in the temperature range (-40 and $+100$ °C). The offset voltage within ± 3% of the supply voltage maintains a wide dynamic range regardless of changes in the ambient temperature. The measured THD at 10 Hz and 2 kHz was ≥ 55 dB in the temperature range from -40 to $+100$ °C. The evaluations during the temperature tests show that the chopper ASIC preamplifier using PTAT circuits can operate over a wide temperature range under harsh space environments. In addition, plasma wave instruments are required not only for high stability for wide temperature variations, but also high radiation tolerance. The radiation tolerance of each circuit block in the chopper ASIC preamplifier is ≥ 200 krad from previous radiation exposure tests (Tokunaga et al. 2020) using the same circuit components. Radiation exposure tests using actual bare chips are a future work, but the chopper ASIC preamplifier can be insensitive to radiation environments based on the previous experiments for the circuit components in the ASIC chip.

Conclusion
Although chopper-stabilized amplifiers have excellent noise characteristics, their large circuit size makes them unsuitable for onboard satellite applications with resource constraints (size, mass, and power, etc.), but these problems are solved by ASIC technology. We developed a chopper-stabilized ASIC preamplifier for improving the NEMI of an SC in the frequency range from 100 mHz to 100 Hz, and analyzed an equivalent circuit model for obtaining the NEMI. By chopping the input signal, the equivalent input noise at 100 mHz is decreased by approximately 21 dB in comparison with that of a low noise ASIC preamplifier in stage (ii). We evaluated the NEMI of two SCs with lengths of 20 and 5 cm. The NEMI values are acceptable for probing typical plasma waves from 100 mHz to 4 kHz. We confirmed that the measured NEMI results of both SCs with the chopper ASIC preamplifier were in good agreement with the calculation results by Eq. (9) using the equivalent circuit model in Fig. 3. The temperature stability of the chopper ASIC preamplifier showed good performance with low temperature variations within 2.0 dB for the gain as a benefit using PTAT circuits. The chopper ASIC preamplifier consisting of rad-hard ASICs can operate under high-radiation environments. It is concluded from these results that the chopper ASIC preamplifier with high robustness for space environments improves NEMI from 100 mHz to several 10 Hz. However, the chopper ASIC preamplifier only probes plasma waves up to 4 kHz in this prototype. We will extend the detectable frequency range of plasma waves by improving the gain band width product of the ASIC preamplifier in stage (ii). The developed chopper ASIC preamplifier will contribute to plasma wave observations for improved understanding magnetospheric dynamics in future missions.

Abbreviations

ASIC	Application-specific integrated circuit
CMOS	Complementary metal oxide semiconductor
NEMI	Noise equivalent magnetic induction
SC	Search coil

Author contributions
MO led the development of the chopper ASIC preamplifier and significantly contributed to the manuscript drafting. YT manufactured, measured, and analyzed the ASIC, and drafted the original manuscript. HK evaluated a prototype of chopper amplifier. SY substantially contributed to data analysis and interpretation. All authors read and approved the final manuscript.

Availability of data and materials
The measurement data and the developed ASIC chips that support the findings of this study are available from the corresponding author upon reasonable request.

Ozaki *et al. Earth, Planets and Space*   (2023) 75:84

Page 11 of 11

Declarations

Ethics approval and consent to participate
Not applicable.

Consent for publication
Not applicable.

Competing interests
The authors declare no competing interests.

Author details
[1]Kanazawa University, Kakuma-Machi, Kanazawa 920-1192, Japan. [2]Present Address: Socionext Inc., Kasugai, Aichi, Japan.

References

Angelopoulos V, Tsai E, Bingley L et al (2020) The ELFIN mission. Space Sci Rev 216:103. https://doi.org/10.1007/s11214-020-00721-7

Baker DN (2021) Wave–particle interaction effects in the Van Allen belts. Earth Planets Space 73:189. https://doi.org/10.1186/s40623-021-01508-y

Brokaw AP (1974) A simple three-terminal IC bandgap reference. IEEE J Solid State Circuits 9(6):388–393. https://doi.org/10.1109/JSSC.1974.1050532

Fukuhara H et al (2012) Tiny waveform receiver with a dedicated system chip for observing plasma waves in space. Meas Sci Technol 23:10. https://doi.org/10.1088/0957-0233/23/10/105903

Johnson AT et al (2020) The FIREBIRD-II CubeSat mission: focused investigations of relativistic electron burst intensity, range, and dynamics. Rev Sci Instrum 91:034503. https://doi.org/10.1063/1.5137905

Kojima H et al (2010) Miniaturization of plasma wave receivers onboard scientific satellites and its application to the sensor network system for monitoring the electromagnetic environments in space. Adv Geosci 2010:461–481

Magnes W et al (2008) Highly integrated front-end electronics for spaceborne fluxgate sensors. Meas Sci Technol 19:11. https://doi.org/10.1088/0957-0233/19/11/115801

Matsuoka A, Teramoto M, Nomura R et al (2018) The ARASE (ERG) magnetic field investigation. Earth Planets Space 70:43. https://doi.org/10.1186/s40623-018-0800-1

Omura Y (2021) Nonlinear wave growth theory of whistler-mode chorus and hiss emissions in the magnetosphere. Earth Planets Space 73:95. https://doi.org/10.1186/s40623-021-01380-w

Ozaki M et al (2014) Current-sensitive CMOS preamplifier for investigating space plasma waves by magnetic search coils. IEEE Sens J 14(2):421–429. https://doi.org/10.1109/JSEN.2013.2284011

Ozaki M et al (2016) Development of an ASIC preamplifier for electromagnetic sensor probes for monitoring space electromagnetic environments. Earth Planets Space 68:91. https://doi.org/10.1186/s40623-016-0470-9

Ozaki M, Yagitani S, Kasahara Y et al (2018) Magnetic search coil (MSC) of plasma wave experiment (PWE) aboard the Arase (ERG) satellite. Earth Planets Space 70:76. https://doi.org/10.1186/s40623-018-0837-1

Ozaki M, Shiokawa K, Kataoka R et al (2022) Localized mesospheric ozone destruction corresponding to isolated proton aurora coming from Earth's radiation belt. Sci Rep 12:16300. https://doi.org/10.1038/s41598-022-20548-2

Rhouni A, Sou G, Leroy P, Coillot C (2013) Very low 1/f noise and radiation-hardened CMOS preamplifier for high-sensitivity search coil magnetometers. IEEE Sens J 13(1):159–166. https://doi.org/10.1109/JSEN.2012.2211347

Sordo-Ibáñez S et al (2015) A front-end ASIC for a 3-D magnetometer for space applications by using anisotropic magnetoresistors. IEEE Trans Magn 51:1. https://doi.org/10.1109/TMAG.2014.2356976

Teng S, Li W, Tao X, Ma Q, Wu Y, Capannolo L et al (2019) Generation and characteristics of unusual high frequency EMIC waves. Geophys Res Lett 46:14230–14238. https://doi.org/10.1029/2019GL085220

Tokunaga Y et al (2020) ASIC waveform receiver with improved environmental tolerance for probing space plasma waves in environments with high radiation and wide temperature variation. URSI Radio Sci Bull 372:12–21. https://doi.org/10.23919/URSIRSB.2020.9240097

Walsh BM, Collier MR, Atz E, Billingsley L, Broll JM, Connor HK et al (2021) The cusp plasma imaging detector (CuPID) cubesat observatory: mission overview. J Geophys Res Space Phys 126:e2020JA029015. https://doi.org/10.1029/2020JA029015

Xu J et al (2013) Measurement and analysis of current noise in chopper amplifiers. IEEE J Solid State Circuits 48(7):1575–1584. https://doi.org/10.1109/JSSC.2013.2253217

Yan B, Zhu W, Liu L, Liu K, Fang G (2014) Equivalent input magnetic noise analysis for the induction magnetometer of 0.1 mHz to 1 Hz. IEEE Sens J 14(12):4442–4449. https://doi.org/10.1109/JSEN.2014.2336971

Zushi T et al (2015) Small sensor probe for measuring plasma waves in space. Earth Planets Space 67:127. https://doi.org/10.1186/s40623-015-0298-8

Publisher's Note

Springer Nature remains neutral with regard to jurisdictional claims in published maps and institutional affiliations.